Analytical Design Methodology for Litz-Wired High-Frequency Power Transformers

Ernesto L. Barrios, *Student Member, IEEE*, Alfredo Ursúa, *Member*, *IEEE*, Luis Marroyo, *Member*, *IEEE*, and Pablo Sanchis, *Senior Member, IEEE*

***Abstract*— In the last quarter of a century, high-frequency transformer design has been one of the major concerns to power electronics designers in order to increase converter power densities and efficiencies. Conventional design methodologies are based on iterative processes and rules of thumb founded more on expertise than on theoretical developments. This paper presents an analytical design methodology for litz-wired high-frequency power transformers that provides a deep insight into the transformer design problem making it a powerful tool for converter designers. The most suitable models for the calculation of core and winding losses and the transformer thermal resistance are first selected and then validated with a 5 kW 50 kHz commercial transformer for a PV application. Based on these models, the design methodology is finally proposed, reducing the design issue to directly solving a five-variable non-linear optimization problem. The methodology is illustrated with a detailed design in terms of magnetic material, core geometry and primary and secondary litz wire sizing. The optimal design achieves a 46.5% power density increase and a higher efficiency of 99.70% when compared to the commercial one.**

***Index Terms*— Analytical design methodology, high-frequency transformers, litz wire, PV power electronic converters.**

I. Introduction

HIGH-FREQUENCY (HF) power transformers with rated powers from 1 to about 25 kVA are traditionally used in AC/DC high power supplies such as microwave heating, telecom and uninterruptible power supplies [1], [2]. They operate in the 10-200 kHz frequency range and have a high enough surface to volume ratio to obtain high power densities with free cooling. The increase in distributed generation from renewable sources, the development of electric and hybrid vehicles, and the emergence of SiC devices has drawn the attention to these transformers, and particularly to their design, due to their advantages over the line-frequency ones, such as higher power densities and efficiencies, and lower costs [3]-[7].

Manuscript received March 17, 2014; revised June 13, 2014; accepted July 25, 2014.

This work was supported in part by the Spanish Ministry of Economy and Competitiveness under Grants DPI2010-21671-C02-01 and DPI2013-42853-R and by the Public University of Navarra.

The authors are with the Department of Electrical and Electronic Engineering, Public University of Navarra, Pamplona, Spain (e-mail: ernesto.barrios@unavarra.es; alfredo.ursua@unavarra.es; luisma@unavarra.es; pablo.sanchis@unavarra.es).

Initial design specifications for a transformer are the rated power S, rms-voltage V_{rms}, frequency f, transformer turns ratio n, and maximum ambient temperature τ_{amb_max}. Together with the specifications, the design criteria have to be established, usually in terms of maximum efficiency and minimum volume. The design constraints are mainly physical or given by the manufacturing environment. The first physical constraint is Faraday's law:

$$V_{rms} = 4 \cdot k_{sh} \cdot N \cdot f \cdot B_p \cdot A_c \quad (1)$$

where k_{sh} is the waveform factor of the applied voltage waveform, N the number of turns, B_p the magnetic induction amplitude and A_c the cross-sectional area of the magnetic core. The second constraint is the thermal limit:

$$R_{th} \cdot P_t \leq \Delta\tau_{\max} \quad (2)$$

where R_{th} is the transformer thermal resistance, P_t is the total power loss and $\Delta\tau_{\max}$ the maximum permitted temperature rise**.** The third constraint is the transformer turns ratio between the primary and secondary number of turns, N_p and N_s:

$$n = N_p / N_s \,. \quad (3)$$

The fourth one is a geometric constraint, which establishes that windings must fit into the limited core window area A_w. Finally, the manufacturing environment determines the material availability to cost ratio. The design process must result in an optimal design regarding the magnetic material and shape, the type and disposition of the windings, and the number of turns.

Due to the large number of degrees of freedom, conventional transformer design methodologies are based on iterative procedures. These design methodologies can be split into two groups: pure iterative methodologies [8]-[10] and rules-of-thumb-based iterative methodologies [1], [11]-[20]. Pure iterative methodologies face the design problem by covering particular ranges of several design variables until a feasible design is obtained. The methodologies of the second group are most commonly used since they speed up the iterative process by using rules of thumb to set the starting values for some variables. These rules of thumb are assumptions justified by expertise that make it possible to simplify the design problem. The most common are:

1) *Core selection.* The magnetic core power-handling ability is evaluated solely by means of its area product [11], [13]-[15], [18], [20], or its geometric-constants [15], [20]. In both cases the values for the current density amplitude J_p and B_p are established beforehand.

2) *Power loss distribution*. The core loss is set equal to the winding loss [14], [15].
3) *Litz wire sizing.* A strand diameter lower than the skin depth is established and then the extra ac power loss is either disregarded [14], [15], or considered constant in the rest of the design procedure [1], [11], [20].
4) *Other rules of thumb.* Primary and secondary winding copper losses are equalized [11], [13]. The window area is distributed equally between primary and secondary windings [11]. Only one magnetic material is taken into account in the design process [18].

Some of these rules of thumb have already been rejected through theoretical developments. In the case of the first one, it has been recently demonstrated that the shape of the core has a strong influence on the design problem [16], [19]. Regarding the power loss distribution, it has been demonstrated that the optimal relation between core and copper losses depends on the characteristics of the magnetic material [1], [11], [16]-[18]. Furthermore, the iterative characteristic of conventional design methods complicates the optimization of the power converter since, in order to analyze the influence of a change in the converter magnitudes on the transformer, the entire design process must be repeated. This is the case when analyzing the dependence of the power density on the switching frequency [13], [16].

The aim of this paper is to propose a novel analytical HF power transformer design methodology that includes the complex multi-physical dependency between the transformer design variables, and directly leads to an overall optimal design including the core shape and material, litz wire sizes, and winding distribution. In Sections II, III and IV, existing models of the core loss [21]-[24], litz wire winding loss [22]-[31], and transformer thermal behavior [1], [11], [12], [14], [15], [35], [36] are reviewed and selected. In Section V, the selected models are used to characterize a commercial litz-wired HF transformer and validated through dedicated experimental tests. After defining in Section VI the design problem through a set of design parameters, the methodology is proposed in Section VII. In Section VIII, the methodology is applied to a real-world design example and a global optimal design is obtained.

II. Magnetic Modeling

A. Core Loss

Core loss can be calculated using hysteresis models, loss separation models and empirical models [17]. Hysteresis and separation models, also known as theoretical models, are complex since they require extensive measurements and parameter extractions that hinder their application in design procedures. Furthermore, the accuracy obtained does not justify their complexity. On the contrary, empirical methods obtain similar accuracy but are easy to calculate from the information provided by manufacturers [1]. Thus, in practical transformer design, these methods are normally used. The first empirical method to calculate core loss density p_c was the well-known original Steinmetz equation (OSE) [12], [21]:

$$p_c = C_m \cdot f^x \cdot B_p{}^y \cdot \left(c_{T2} \cdot \tau_{ope}^2 - c_{T1} \cdot \tau_{ope} + c_{T0}\right) \quad (4)$$

where f is the frequency of the magnetic induction, τ_{ope} is the operating temperature, C_m, x, and y are the loss coefficients, and c_{T2}, c_{T1} and c_{T0} are the temperature coefficients. These coefficients, that empirically model the power loss dependence on both the magnetic material operating point (f, B_p) and τ_{ope}, are specified by the manufacturers.

Expression (4) is only valid for sinusoidal remagnetization, which is not normally found in power electronics. Therefore, it needs to be modified for arbitrary magnetizing current waveforms. Several models have been developed over the last 15 years including the modified Steinmetz equation (MSE) first introduced in [22], the generalized Steinmetz equation (GSE), the improved GSE (iGSE), the natural Steinmetz extension, the equivalent elliptical loop, the waveform coefficient Steinmetz equation [23] and the improved iGSE (i^{2}GSE) [24]. All of them are based on the OSE approach but including variations based on different physical interpretations of the dynamic remagnetization process. HF power transformers used in typical power converters have square input voltages with or without zero periods. In these cases, the MSE, the iGSE and the i^{2}GSE have been shown to be the most accurate core loss models [18], [23], [24]. Each model improves the accuracy of the previous one but with the drawback of increasing complexity. For the purpose of designing HF transformers, the MSE represents a satisfactory tradeoff between simplicity and accuracy, and is therefore used in this paper for the calculation of core loss P_c as [22]:

$$P_c = \frac{1}{T} C_m \cdot f_{eq}{}^{(x-1)} \cdot B_p{}^y \cdot \left(c_{T2} \cdot \tau_{ope}^2 - c_{T1} \cdot \tau_{ope} + c_{T0}\right) \cdot V_c \quad (5)$$

where T is the period of the magnetic induction waveform, V_c the magnetic core volume, and f_{eq} is the equivalent frequency that represents the average remagnetization velocity:

$$f_{eq} = \frac{2}{\Delta B^2 \cdot \pi^2} \int_0^T \left(\frac{dB}{dt}\right)^2 dt \,. \quad (6)$$

B. Soft Magnetic Materials and Core Geometry

In HF applications, soft magnetic materials are used due to their low power loss. They are classified into two groups: *ferromagnetic*, which are iron alloys such as nanocrystalline and amorphous materials; and *ferrimagnetic*, such as ferrites. Table I shows the characteristics provided by the manufacturers for the main soft magnetic materials suitable for power applications. This table includes the material type, grade, and manufacturer, as well as the saturation magnetic induction at 100 °C, B_{sat100}, and the core loss coefficients for the indicated frequency ranges. Concerning core geometry, U and E cores are commonly used in power applications due to their modularity and availability for a wide range of sizes [15]. As shown in Fig. 1, their geometry is characterized by four characteristic dimensions: mean magnetic path l_c, cross-sectional area A_c, window area A_w and core volume V_c.

TABLE I POWER SOFT MAGNETIC MATERIALS PROPERTIES

Material type		Mn-Zn Power Ferrites[a]			Nanocrys-talline	Amor-phous
Material grade		3C94	R	N87	FT-3M	2705M
Manufacturer		Ferrox-cube	Magne-tics	Epcos	Hitachi	Metglas
B_{sat100} (T)		0.35	0.35	0.35	0.8	0.55
f range (kHz)		20-200	<200	20-200	<500	<500
Steinmetz Coefficients	C_m ($\cdot 10^{-4}$)	23.7	26.9	19	1.1	0.1
	x	1.46	1.43	1.41	1.62	1.88
	y	2.75	2.85	2.57	1.98	2.21
	c_{T2} ($\cdot 10^{-4}$)	1.65	1.75	4.25	0	0
	c_{T1} ($\cdot 10^{-2}$)	3.1	3.42	8.91	0	0
	c_{T0}	2.45	2.67	5.67	1	1

[a] Minimum power loss at 90-100 °C

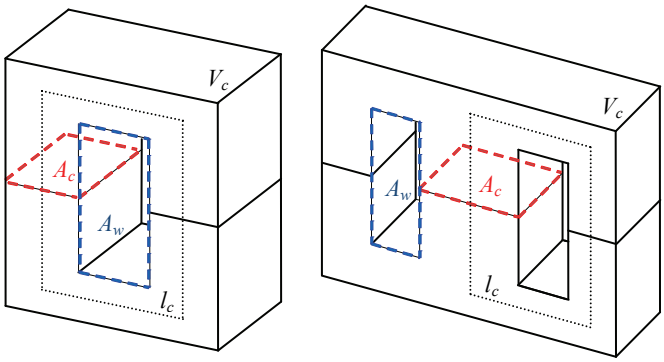

Fig. 1. Characteristic dimensions l_c, A_c, A_w and V_c for U and E cores.

III. WINDING MODELING

When working at high frequencies, litz wires are used to minimize copper loss. Litz wires consist of N_0 strands of radius r_0 isolated and parallel connected at the wire's beginning and end. When a single litz wire conducts time-varying currents, the well-known skin and internal proximity effects can cause a non-uniform current distribution. The skin effect forces the current to flow close to the surface in each strand. It is characterized by the skin depth δ:

$$\delta = \frac{1}{\sqrt{\pi \cdot \sigma \cdot f \cdot \mu}} \tag{7}$$

where μ and σ are the magnetic permeability and the electrical conductivity of the conductor material, respectively. The internal proximity effect is due to the interaction between each strand and the external magnetic field created by the currents flowing through the rest of strands. Both effects can lead to an increase in the copper loss [25].

When litz wires are wound around a magnetic material and stacked to form windings, a third effect called external proximity effect appears that complicates the calculation of the ac copper loss. In the windings, each turn of the litz wire is located in an external three-dimensional time-varying magnetic field generated by the currents conducted by the rest of wires. This field intensifies eddy currents and can increase winding loss. In order to reduce the magnetic field strength in the window space and, consequently the power loss, windings are sectioned and interleaved. Primary and secondary windings are divided into sections of m_p and m_s layers, respectively, each layer containing b_p and b_s number of turns.

Litz wire winding loss calculation methods can be classified into two major groups: numerical field calculation methods [26], [27], and analytical methods [28]-[32]. Although the first methods make it possible to precisely calculate the winding loss, they are disproportionately time-consuming when applied to litz wire windings. On the contrary, the analytical methods are easy-to-use and, in HF power transformers, where there are no air gaps and the strand radius remains below the skin depth, they present good accuracy. Thus, for the purpose of designing, analytical methods are recommended.

The analytical methods can, in turn, be divided into three groups. The methods of the first group calculate the power loss using the complex permeability of a conductor matrix concept [28]. These methods provide a good accuracy even at high r_0/δ values, but their implementation is complicated since the real and imaginary parts of the winding permeability have to be correctly determined. The second group [29], [30] is based on Dowell's approach [33] and its interpretations including the orthogonality principle presented by Ferreira in [34]. To apply the one-dimensional Dowell's method to litz wire winding, each layer of strands is considered to be equivalent to an individual solid layer of thickness $2r_0$ through the application of a porosity factor. Finally, the methods of the third group extend the stand-alone litz wire loss analysis presented in [25] to the entire winding [31], [32]. Both second and third groups lead to similar results with a good tradeoff between simplicity and accuracy [29], [32]. As the physical phenomena are more accurately modeled by the methods of the third group, the Tourkhani model [32] is adopted in this paper, and its approximation for $r_0 \leq \delta$ is used, since it can be directly applied to calculate the total winding loss $P_{w,m}$ of a section of m layers as follows:

$$P_{w,m} = R_{dc} \cdot I_{rms}^2 \cdot \left\{1 + \frac{\pi^2 N_0 \beta}{3 \cdot 2^6}\left(16m^2 - 1 + \frac{24}{\pi^2}\right) \cdot \left(\frac{r_0}{\delta}\right)^4\right\}$$
$$= R_{dc} \cdot I_{rms}^2 \cdot F_{ac} \tag{8}$$

where I_{rms} is the rms current, β is the fill factor, that is, the quotient between copper and winding area, F_{ac} is the ac copper loss factor and R_{dc} is the dc resistance:

$$R_{dc} = \frac{MLT_w \cdot N}{\pi \cdot \sigma \cdot r_0^2 \cdot N_0} \tag{9}$$

with MLT_w being the mean length turn of the winding.

IV. THERMAL MODELING

The steady state transformer thermal resistance can be estimated by means of theoretical and empirical models. There exists a wide variety of theoretical thermal models depending on the heat transfer mechanisms considered and their interpretation [1], [11], [12], [14], [15], [35]. Regarding the empirical models, previous work of magnetic material manufacturers have shown that it is possible to establish, for a fixed temperature rise, an empirical formula to model the transformer thermal resistance as a function of its core volume [36]. Empirical models are claimed to obtain similar accuracy to theoretical models but with a much lower complexity [1], [15]. Thus, in this paper, next empirical resistance R_{th} is used,

according to the data provided by the manufacturers for different double E and double U cores, and a temperature increase of 50 °C [36]:

$$R_{th} = \frac{1}{10^{1.34} \cdot V_c^{0.52}} \approx \frac{0.0457}{\sqrt{V_c}}. \quad (10)$$

V. Transformer Model Validation

The selected transformer model is now applied to characterize a commercial 50 kHz 5 kW transformer used in a PV grid connected system. The transformer, whose characteristics are shown in Tables II and VIII, is located in a half bridge ZCS HF resonant intermediate conversion stage.

TABLE II Commercial Transformer Characteristics

S/f	5kW / 50kHz	Magnetic material	CF 139
V_p	215 V	Core	2xEE71/33/32
N_p / N_s	10 / 16	B_p	0.077 T

Core loss is estimated by means of (5). Winding loss for the fundamental $P_{w,50}$ and the third $P_{w,150}$ current components are calculated using (8). The approximation is valid in this case up to the 14th harmonic. The steady state operating temperature τ_{ope} is estimated by means of an iterative process in which the empirical thermal resistance in (10) is used. Fig. 2 shows the test bench. Through dedicated test τ_{ope}, P_c, $P_{w,50}$ and $P_{w,150}$ are measured separately [37]. Measured and estimated values are compared in Table III for different operating powers P at an ambient temperature of 25°C.

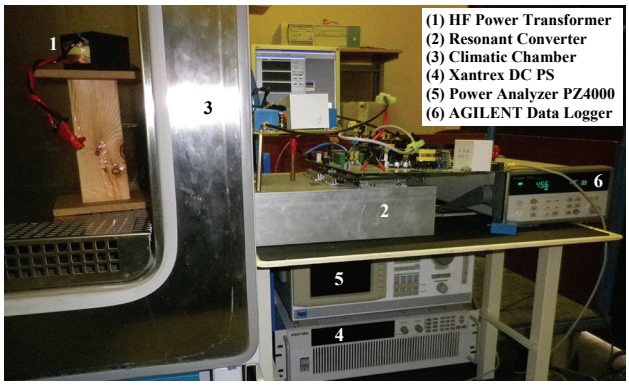

Fig. 2. Test bench used in the HF transformer characterization.

TABLE III Transformer Estimated and Experimental Operation

P	Estimated					Experimental				
	P_c	$P_{w,50}$	$P_{w,150}$	τ_{ope}	R_{th}	P_c	$P_{w,50}$	$P_{w,150}$	τ_{ope}	R_{th}
(kW)	(W)	(W)	(W)	(°C)	(°C/W)	(W)	(W)	(W)	(°C)	(°C/W)
1	5.5	0.5	0.1	46.4	3.5	6.4	0.5	0.1	50.1	3.6
2	5.1	2.3	0.3	50.5	3.5	5.9	1.9	0.2	54.0	3.6
3	4.3	4.6	0.6	58.6	3.5	5.1	4.3	0.4	59.8	3.6
4	3.5	8.3	1.1	69.5	3.5	4.2	7.9	0.8	70.6	3.6
5	2.6	13.2	1.6	85.8	3.5	3.4	13.1	1.2	85.2	3.4

As shown in Table III, estimated and experimental results are in good agreement. Winding loss model is accurate with a slight overestimation of losses. Core loss estimation is less accurate due to the uncertainty introduced by the lack of information about the thermal characteristic of the ferrite used. The thermal model is also accurate, with good agreement between estimated and measured temperatures. The small deviations in the temperature at low operating powers are due not to the thermal model but to the errors in the estimation of P_c. As a conclusion, for the purpose of transformer designing, the use of the modified Steinmetz equation, the Tourkhani winding loss model and the empirical thermal model is justified due to their tradeoff between simplicity and accuracy.

VI. Design Problem Definition

A. Core Geometry Modeling

Similarly to the homothetic analysis carried out in [16], the core geometry of the two main core types is completely described in Fig. 3 through four parameters: the dimensional factor a in meters, and the three non-dimensional shape coefficients $c1$, $c2$ and $c3$. The core characteristic dimensions can be defined now as a function of these parameters as shown in Table IV. MLT_c is the core mean length turn defined as the length of a turn wound at the middle of the window width, and V_e is the transformer equivalent volume that represents the volume including the windings. These two characteristic dimensions depend not only on the core type, like the rest of dimensions, but also on the way the windings are wound. In Table IV, the most common ways to wind are considered, which are over the central leg "shell type" for double E or EE, and over both legs for double U or UU cores. In the fourth column, the dimensions are expressed in a generic form in which the non-dimensional core characteristic coefficients a_c, a_w, v_c, mlt, and v_e are solely function of the shape coefficients.

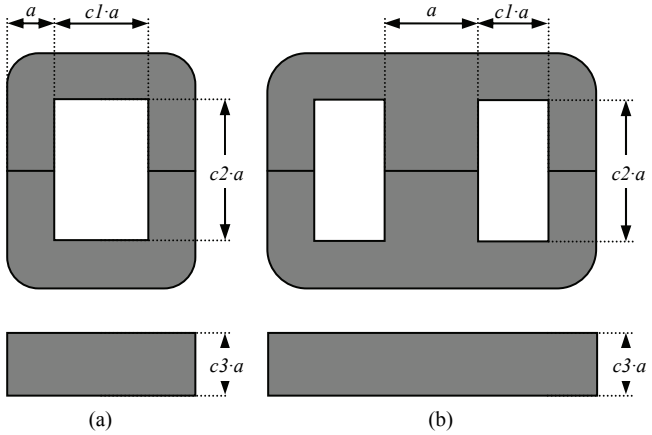

Fig. 3. Dimensional factor a and shape coefficients $c1$, $c2$, and $c3$, of the two main types of power cores: (a) double U and (b) double E.

TABLE IV Characteristic Dimensions of EE and UU Cores

Characteristic dimensions	Both legs double U	Shell type double E	Generic form
A_c	$c3 \cdot a^2$	$c3 \cdot a^2$	$a_c \cdot a^2$
A_w	$c1 \cdot c2 \cdot a^2$	$c1 \cdot c2 \cdot a^2$	$a_w \cdot a^2$
V_c	$2c3(c1+c2+2)a^3$	$2c3(c1+c2+5/4)a^3$	$v_c \cdot a^3$
MLT_c	$2 \cdot (c1+c3+1) \cdot a$	$2 \cdot (2 \cdot c1+c3+1) \cdot a$	$mlt \cdot a$
V_e	$2 \cdot (c1+1) \cdot (c2+2) \cdot (c3+c1) \cdot a^3$	$2 \cdot (c1+1) \cdot (c2+1) \cdot (c3+2 \cdot c1) \cdot a^3$	$v_e \cdot a^3$

Including this analysis, the core loss can be now expressed as follows:

$$P_c = K_1 a^3 B_p^{\ y} \quad (11)$$

where coefficient K_1 is:

$$K_1 = 1000 \cdot k_{mag} \cdot C_m \cdot f^x \cdot v_c \cdot \left(c_{T2} \cdot \tau_{ope}^2 - c_{T1} \cdot \tau_{ope} + c_{T0}\right) \quad (12)$$

where k_{mag} is the core loss waveform coefficient that relates the loss with the actual magnetic induction to the loss with sinusoidal waveform. For two- and three-level voltage profiles, typical of isolated dc-dc power applications, k_{mag} can be expressed as a function of the length of the zero-voltage period θ in rad as follows [23]:

$$k_{mag} = \left(\frac{8}{\pi^2}\right)^{x-1} \cdot \left(1 - \frac{\theta}{\pi}\right)^{y-x-1} . \quad (13)$$

B. Litz Wire Winding Geometry and Loss

The design parameters of a litz wire are the strand radius r_0 and the number of strands N_0. These parameters are not independent since the available area for the winding is limited [29]. For a given area, as the strands are insulated, the fill factor β depends on the combination between r_0 and N_0. The dependency between the strand insulation thickness g and r_0 for a 0.2-0.01 mm range can be modeled from PACK Feindrähte litz wire manufacturer's data [38] as:

$$g(r_0) = 0.484 \cdot r_0 + 2 \times 10^{-6} . \quad (14)$$

An approximation for lower radii can be found in [29]. The dependence of N_0 on r_0 for a circular wire, when a number of turns N has to be fitted in an available winding area $A_{a,w}$, can then be expressed as:

$$N_0 = \frac{K_d \cdot A_{a,w}}{N \cdot \pi \cdot (r_0 + g(r_0))^2} = \frac{K_d \cdot A_{a,w}}{N \cdot \pi \cdot (e_1 \cdot r_0 + e_2)^2} \quad (15)$$

where e_1 and e_2 are the litz wire insulation constants, and K_d is a constant winding factor that models the reduction of the available area due to factors such as serving, strand packing, bundle filler and packing, twist and turn packing [29]. The analysis of the window area distribution complicates the design procedure since it can only be made in a discrete way, i.e. the number of turns forming a layer must be an integer. This makes it necessary to follow a trial and error procedure to fill the window [19]. In this paper, and to prevent this discontinuity from obstructing the design problem analysis, the complete window area is initially assigned to the windings. If litz wires are correctly sized, the window area needs to be completely filled [29]. Therefore, the number of turns per layer b can be related directly to the window dimensions and the litz-wire characteristics as follows:

$$b = \frac{c_2 \cdot a \cdot \sqrt{K_d}}{2 \cdot \sqrt{N_0} \cdot (e_1 \cdot r_0 + e_2)} . \quad (16)$$

In addition, the fill factor β of a winding made up of N turns of a litz wire with N_0 strands of radius r_0 can be expressed as:

$$\beta = \frac{N \cdot \pi \cdot r_0^{\,2} \cdot N_0}{A_{a,w}} = \frac{K_d \cdot r_0^{\,2}}{(e_1 \cdot r_0 + e_2)^2} \quad (17)$$

where N_0 has been expressed as a function of r_0 by applying (15). As an equal window distribution between primary and secondary is not justified [1], [20], primary and secondary winding areas, A_{wp} and A_{ws}, can be referred to the window area A_w through the winding distribution coefficient α as:

$$A_{wp} = \alpha \cdot A_w = \alpha \cdot a_w \cdot a^2 , \quad (18)$$

$$A_{ws} = (1-\alpha) \cdot A_w = (1-\alpha) \cdot a_w \cdot a^2 . \quad (19)$$

Two winding dispositions have now to be distinguished. If maximum efficiency is desired, primary and secondary windings must be fully interleaved as shown in Fig. 4. However, in some cases, primary and secondary windings cannot be interleaved. For instance, in high voltage applications, they are grouped into separate chambers due to isolation concern. When leakage inductance and interwinding capacitance are used as filter [39] or resonant [40] components, a non-interleaved structure is also preferred. Loss calculation is carried out below for both winding dispositions:

1) Maximum efficiency winding interleaving. As shown in Fig. 4, the primary and secondary number of layers, m_p and m_s, are equal to the unit. The primary and secondary windings are divided, respectively, into p_p and p_s sections of one layer with b_p turns per primary layer and b_s turns per secondary layer. Applying (8) to each primary winding section and adding the losses for each section, the total primary winding loss P_{wp} are expressed as:

$$P_{wp} = \frac{N_p \cdot I_{p,rms}^2}{\pi \cdot \sigma \cdot r_{0p}^2 \cdot N_{0p}} \cdot F_{ac} \cdot \frac{\sum_{j=1}^{p_p} MLT_j}{p_p} \quad (20)$$

where MLT_j is the mean length turn of layer j. The average of the mean length turns of the different layers can be approximated by the core mean length turn MLT_c. Introducing (15), (17) and (18) in (20), the primary winding power loss is:

$$P_{wp} = MLT_c \cdot N_p^2 \cdot I_{p,rms}^2 \cdot \left(\frac{(e_1 \cdot r_{0p} + e_2)^2}{A_w \cdot K_d \cdot \sigma \cdot \alpha \cdot r_{0p}^2} + \frac{2\sqrt{2} \cdot K_d \cdot \sigma \cdot \mu^2 \cdot f^2}{N_p} \cdot \frac{r_{0p}^4}{(e_1 \cdot r_{0p} + e_2)^2} \right) . \quad (21)$$

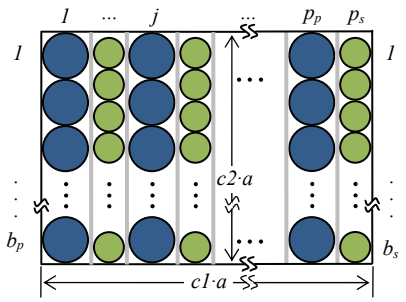

Fig. 4. Generic maximum efficiency interleaved windings distribution.

The secondary winding loss P_{ws} can be derived similarly. By expressing N_s and the secondary current I_s in terms of N_p and I_p with the turns ratio, and adding P_{wp} and P_{ws}, the total winding loss P_w can be obtained. Particularizing now (1) for the primary, N_p can be expressed as a function of B_p. Finally, the core characteristic dimensions can be expressed in their generic form as indicated in Table IV and then included in the expression for the winding losses as follows:

$$P_w = \frac{K_2}{a^5 {B_p}^2}\left(\frac{\left(e_1 r_{0p}+e_2\right)^2}{\alpha {r_{0p}}^2}+\frac{\left(e_1 r_{0s}+e_2\right)^2}{(1-\alpha){r_{0s}}^2}\right) + \frac{K_3}{aB_p}\left(\frac{{r_{0p}}^4}{\left(e_1 r_{0p}+e_2\right)^2}+\frac{n\cdot {r_{0s}}^4}{\left(e_1 r_{0s}+e_2\right)^2}\right) \quad (22)$$

where r_{0p} and r_{0s} are the primary and secondary radii. Coefficients K_2 and K_3 are:

$$K_2 = \frac{{V_{p,rms}}^2 \cdot {I_{p,rms}}^2}{16\cdot {k_{sh}}^2\cdot\sigma\cdot f^2}\cdot\frac{mlt}{a_c^2\cdot a_w\cdot K_d}, \quad (23)$$

$$K_3 = \frac{V_{p,rms}\cdot {I_{p,rms}}^2\cdot f\cdot\sigma\cdot\mu^2}{\sqrt{2}\cdot k_{sh}}\cdot\frac{mlt\cdot K_d}{a_c}. \quad (24)$$

where the waveform factor k_{sh} is equal to 1 for a square voltage and 1.11 when the voltage is sinusoidal [18].

2) Non-interleaved windings. In this case, the number of layers per section is not required to be equal to the unity. In addition, primary and secondary mean length turn, MLT_p and MLT_s, are not equal anymore and can be expressed for "shell type" double E core type as follows:

$$MLT_p = mlt_p\cdot a = 2\left(2\alpha\cdot c1 + c3 + 1\right)\cdot a, \quad (25)$$

$$MLT_s = mlt_s\cdot a = 2\left(2\left(1+\alpha\right)\cdot c1 + c3 + 1\right)\cdot a. \quad (26)$$

When the windings are not interleaved, the turns of a winding are distributed in m layers of b turns each. Thus, including in (16) the N_0 expression in (15) and the window area distribution between primary and secondary windings modeled in (18) and (19), the squared m_p and m_s can be expressed as:

$$m_p^2 = \left(\frac{N_p}{b_p}\right)^2 = \frac{4\cdot N_p\cdot\alpha\cdot c1}{\pi\cdot c2}, \quad (27)$$

$$m_s^2 = \left(\frac{N_p}{n\cdot b_s}\right)^2 = \frac{4\cdot N_p\cdot(1-\alpha)\cdot c1}{\pi\cdot n\cdot c2}. \quad (28)$$

If the Tourkhani approximation for the calculation of winding losses in (8) is developed for primary and secondary windings in a similar way as done for the maximum efficiency interleaving, but including the dependencies expressed in (25), (26), (27) y (28), next expression for the total winding losses of a non-interleaved two-winding transformer is obtained:

$$P_w = \frac{K_{2,n}}{a^5 {B_p}^2}\left(\frac{mlt_p\left(e_1 r_{0p}+e_2\right)^2}{\alpha\cdot {r_{0p}}^2}+\frac{mlt_s\left(e_1 r_{0s}+e_2\right)^2}{(1-\alpha)\cdot {r_{0s}}^2}\right) + \frac{K_{3,n}}{a^3 B_p^2}\left(\frac{mlt_p\cdot\alpha\cdot {r_{0p}}^4}{\left(e_1 r_{0p}+e_2\right)^2}+\frac{mlt_s\cdot(1-\alpha)\cdot {r_{0s}}^4}{\left(e_1 r_{0s}+e_2\right)^2}\right) + \frac{K_{4,n}}{a\cdot B_p}\left(\frac{mlt_p\cdot {r_{0p}}^4}{\left(e_1 r_{0p}+e_2\right)^2}+\frac{mlt_s\cdot n\cdot {r_{0s}}^4}{\left(e_1 r_{0s}+e_2\right)^2}\right) \quad (29)$$

In this case, coefficients K_2, K_3 and K_4 are:

$$K_{2,n} = \frac{{V_{p,rms}}^2\cdot {I_{p,rms}}^2}{16\cdot {k_{sh}}^2\cdot\sigma\cdot f^2\cdot a_c^2\cdot a_w\cdot K_d}, \quad (30)$$

$$K_{3,n} = \frac{{V_{p,rms}}^2\cdot {I_{p,rms}}^2\cdot\sigma\cdot\mu^2\cdot\pi^2}{48\cdot k_{sh}^2}\cdot\frac{K_d\cdot c1}{a_c^2\cdot c2}, \quad (31)$$

$$K_{4,n} = \frac{V_{p,rms}\cdot {I_{p,rms}}^2\cdot f\cdot\sigma\cdot\mu^2\cdot K_d}{10\sqrt{3}\cdot k_{sh}\cdot a_c}. \quad (32)$$

Finally, when working with nonsinusoidal currents, and both for fully interleaved and for non-interleaved windings, the total winding power loss must include the winding losses due to the current harmonics as follows:

$$P_w = \sum_{i=1}^{n_{\max}} P_{w,i} \quad (33)$$

where $P_{w,i}$ is the copper loss for the current harmonic i and n_{max} is the maximum harmonic considered. For each harmonic, coefficients K_2, K_3, $K_{2,n}$, $K_{3,n}$, and $K_{4,n}$ need to be particularized for the harmonic *rms* current $I_{p,rms,i}$ and frequency f_i.

C. Design parameters

The design characteristic parameters that have to be calculated from the design process are shown in Table V. Each magnetic material implies a particular value for the saturation magnetic induction B_{sat} and a particular set of Steinmetz coefficients. The core size and shape are defined by means of a, $c1$, $c2$, and $c3$. The magnetic material operating point is determined by B_p. The winding distribution is defined by the strand radii r_{0p} and r_{0s}, and the winding distribution factor α. Once these parameters have been determined, the remaining design parameters can be calculated: the number of primary and secondary turns, N_p and N_s, through (1) and (3), the number of primary and secondary strands, N_{0p} and N_{0s}, through (15), and the number of turns per layer through (16).

TABLE V DESIGN CHARACTERISTIC PARAMETERS

Magnetic material	B_{sat}, C_m, x, y
Core type	UU, EE
Core size and shape	a, $c1$, $c2$, $c3$
Magnetic operating point	B_p
Litz wire parameters	r_{0p}, r_{0s}
Window distribution	α

These parameters comprehensively represent the multi-physical nature of the design problem. Conventional design methods usually consider the design problem in terms of fixing B_p and J_p [1], [8]-[20]. However, as the high-frequency electromagnetic effects in the conductors invalidate the constant J_p hypothesis, the proposed methodology does not consider J_p to be a design parameter.

VII. ANALYTICAL DESIGN METHODOLOGY

The requirement for a design to be feasible is that the transformer must be able to dissipate its total loss with a temperature rise equal to or less than the maximum allowable rise $\Delta\tau_{max}$. In addition, transformer design has to deal with two contradictory design criteria, which are minimum volume and maximum efficiency. For the power range considered in this paper, high efficiencies are always obtained due to the low dissipation capacity of free-cooled transformers. Thus, in order to take full advantage of the benefits of operating at high

frequencies, minimizing volume becomes the priority criterion. Introducing (10) in (2), the core volume V_c can be expressed as:

$$V_c \geq \frac{0.0457 \cdot P_t^{1.92}}{\Delta\tau_{\max}^{1.92}}. \quad (34)$$

To minimize V_c, the thermal limit must be transformed into equality. Once equalized (34), minimizing total power loss leads to a minimum volume and then to an optimal design. Thus, from a mathematical point of view, the proposed analytical approach reduces the design problem to minimize the total power loss function subject to the thermal constraint:

$$\begin{aligned} &\min P_t \\ &\text{s.t.} \quad P_t \cdot R_{th} - \Delta\tau_{\max} = 0 \end{aligned} \quad . \quad (35)$$

The optimization problem shown in (35) is a function of the design characteristic parameters defined in Table V. The total loss is the sum of the core losses given by (11) and the winding losses given by (22) in the case of maximum efficiency interleaving and by (29) in the case of non-interleaved windings. Including the core parameterization carried out in Section VI, the empirical expression for R_{th} in (10) can be now rewritten as a function of the factor a as:

$$R_{th} = \frac{0.0457}{v_c^{0.52} \cdot a^{1.56}}. \quad (36)$$

$\Delta\tau_{max}$ is determined by the maximum operating temperature τ_{ope_max} and the maximum permitted ambient temperature τ_{amb_max}. τ_{ope_max} is normally set to about 100 °C [14]. Since the temperature affects both the core and winding losses, the materials' coefficients have to be particularized in the design process for the value of τ_{ope_max} [41].

The resolution of (35) becomes complicated due to the large number of variables involved and the strong nonlinear characteristic of the problem. As there exists only a few soft magnetic materials, which means few possible values for C_m, x, y and B_{sat}, and the shape coefficients $c1$, $c2$ and $c3$ are closely delimited, the proposed solution is then to cover the possible ranges for these coefficients and solve (35) with respect to five design parameters: dimensional factor a, magnetic induction amplitude B_p, primary and secondary strand radii r_{0p} and r_{0s}, and window distribution coefficient α.

The complete design methodology is now presented as a flowchart in Fig. 5. In the first step, the specifications are established. Then, in the second step, the core types and the ranges for $c1$, $c2$ and $c3$ are swept. The optimization problem presented in (35) particularized for the five design parameters is solved in the third step for each core type and shape combination, and for each magnetic material. For a fixed set of core shape coefficients $c1$, $c2$, and $c3$, minimizing the core volume, i.e. minimizing a, is equivalent to minimizing the transformer equivalent volume V_e. Therefore, in the fourth step, from the solutions obtained in the third step, the magnetic material that achieves the lowest value for a is selected. This process is repeated for each core type and shape combination and the selected designs are stored. Finally, when all the core type and shape ranges have been swept, the stored designs are compared in the fifth step and the one with the minimum V_e is selected as the global optimal design.

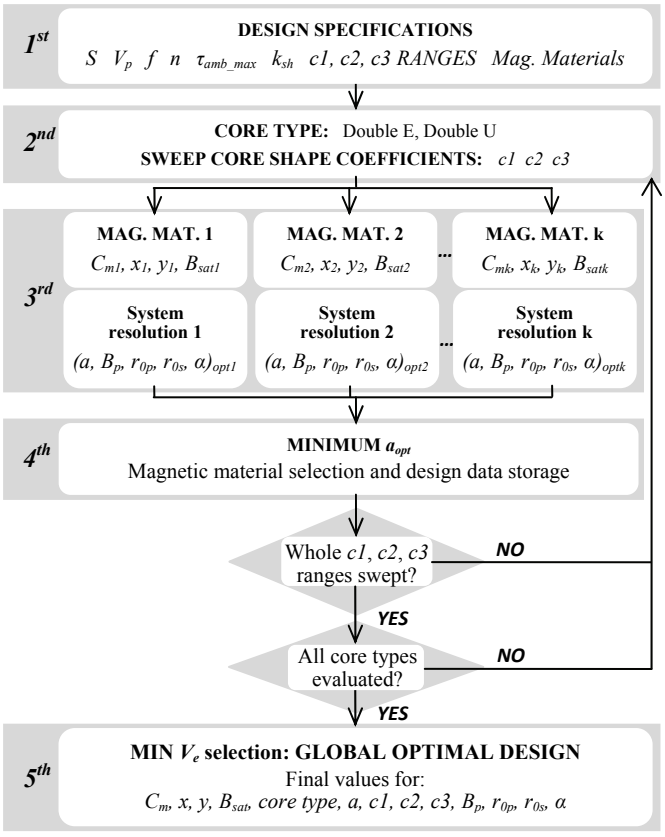

Fig. 5. Analytical design methodology flowchart.

VIII. Design Example

The proposed methodology is now applied to design a high-frequency transformer for the same PV application in Section V. As it is located in a half-bridge ZCS resonant intermediate conversion stage, the applied voltage is a square waveform resulting in a triangular magnetizing current with a constant duty cycle of 0.5. The winding currents, which are the sum of the magnetizing and load currents, are mainly composed of the fundamental and third harmonic components. The worst conditions are considered in the design. Thus, a nominal primary current consisting of a 50 kHz 40.15 A fundamental and a 150 kHz 7.08 A third harmonic is considered. The secondary current has the same waveform but with the transformed amplitude. A maximum ambient temperature of 45 °C, typical of PV systems, and a maximum operating temperature of 100 °C, are considered. Table VI shows the core types, the magnetic materials, the ranges for the core shape coefficients and the winding factor K_d considered in the design.

TABLE VI Design Materials and Core Shapes

Ferrite	3C94, N87	$K_d/e_1/e_2$	$0.6/1.484/2\times10^{-6}$
Nanocrystalline	FT-3M	$c1$ range	0.2-2
Amorphous	2705M	$c2$ range	1-4
Core types	UU, EE	$c3$ range	1-6
Design power	5 kW	$\Delta\tau_{max}$	55 °C

The design methodology described in Fig. 5 is implemented in MATLAB®. The Lagrangian method is used to solve the optimization problem. In this case, the priority is to maximize the efficiency. Therefore, the windings are fully interleaved and expression (22) is used for the winding losses. The theoretical-optimal design characteristics are shown in Table VII. It is interesting to emphasize that the optimal current density J_p, both for primary and secondary conductors, is a quite high value of 7.5 A/mm^2, while the optimal magnetic induction B_p is 0.118 T, quite far from the saturation value.

TABLE VII THEORETICAL-OPTIMAL DESIGN CHARACTERISTICS

Mag. material	FerriteN87	N_p/N_s	5.4/8.6
Core Type	EE	r_{0p}/r_{0s} (mm)	0.036/0.042
c1/*c2*/*c3*	0.4/1.4/3.7	N_{0p}/N_{0s}	1476/688
a (m)	0.0214	α/β	0.501/0.24
B_p (T)/J_p (A/mm^2)	0.118/7.5	P_w/P_c (W)	8/6.05

As a consequence of the analytical nature of the proposed design methodology, an optimal non-integer number of turns is obtained. Thus, the theoretical-optimal design must be adapted by rounding the number of turns to its immediately lower integer in order to obtain a practical optimal design. The practical-optimal design performance at rated power is summarized in Table VIII. The total power loss is the sum of core losses, 7.3 W, and winding losses, 7 W. Primary and secondary winding losses consist of P_{w50} and P_{w150}, that is 6.7 W and 0.33 W, respectively.

The rules of thumb summarized in Section I can now be assessed for the design carried out with the proposed methodology:

1) *Core selection based on the area product A_p.* The expression for A_p is:

$$A_p = A_c \cdot A_w \geq \frac{S}{4 \cdot k_{sh} \cdot \beta \cdot f \cdot J_p \cdot B_p}. \qquad (37)$$

This expression is a necessary condition for a design to be feasible but not a sufficient one as it does not take into account the thermal constraint. The methods based on this rule, establish J_p and B_p beforehand. However, J_p and B_p depend, in turn, on A_p [16]. Since these methods do not take into account the interdependency between these variables, they require a big number of iterations to reach a feasible design that may not necessarily be an optimal one. Evaluating the right term of (37) for the obtained optimal design, it results to be four times lower than the optimal A_p of 43.46 cm^4. That means that, even if the optimal J_p and B_p values were known beforehand and used in (37), the optimal value of A_p, and then the complete optimal design, would still be far from being reached.

2) *Equal power loss distribution.* Contrary to this rule of thumb, the power loss in the theoretical optimal design is not equally distributed between core and windings. As shown in Table VII, their quotient is close to its optimal value of 2/*y* [1], [11], [16]-[18].

3) *Litz wire sizing*. The optimal design makes it possible to determine the optimal values for the primary and secondary litz wires. Traditionally, different rules of thumb are used for litz wire sizing in order to simplify the design problem by fixing the value of the strand radius r_0 to a certain amount of the skin depth δ. In Table VIII, four different litz wire sizing approaches based on common rules of thumb are presented and compared to the optimal design. The approaches are carried out once the required design characteristics (winding arrangement, number of turns and window area) have been fixed by the methodology proposed in this paper.

First approach, named *Litz-wire 1*, only takes into account the skin effect, thus establishing $r_0=\delta$ [11]. Second and third approaches, named *Litz-wire 2* and *Litz-wire 3*, are more common and take $r_0=\delta/3$ [14], [25], and $r_0=\delta/7$ [1], [13], respectively. Finally, the fourth approach, named *Litz-wire 4*, establishes a much more strict relation of $\delta/15<r_0<\delta/30$ [8], [9], [42]. Litz-wire manufacturers usually provide recommended values for r_0 tabulated as a function of the frequency range of operation. Concretely, the New England Wire Technologies advises to use strand radii between the second and third approaches depending on the frequency range [43].

The optimal design, with $r_{0p}\approx\delta/9$ and $r_{0s}\approx\delta/8$, is placed between the third and fourth approaches. Starting from the first approach, the winding losses tend to decrease as the strand radius reduces and its number increases and get close to their optimal value. However, when the number of strands increases over its optimal and the strand radius decreases under the optimal radius, the reduction of the ac factor F_{ac} no longer compensates the increase of the dc resistance R_{dc} and, consequently, the winding losses increase. As shown in Table VIII, the two extreme cases lead to poor designs in terms of losses and temperature. The first approach results in a non-feasible design due to the high temperatures reached. In turn, the fourth approach obtains a more expensive design [44] with a worse performance with respect to the optimal one. This sizing approach is more adequate with higher current harmonic contents or higher number of layers per section cases.

Consequently, the litz wire sizing rules of thumb must not be used as rules of general application because they only lead to good results in specific cases. If the expressions for winding losses (22) and (29) are analyzed together with the design approach in (35), it can be concluded that the optimal litz wire sizing, i.e. the litz wire that leads to minimum transformer volume and maximum efficiency, depends on a large number of factors that change according to the application considered. Some of these factors are current and voltage waveforms, number of layer per section, magnetic core shape and size, the levels of currents and voltages for a given power, materials used, range considered for the strand radius, frequency, or temperature.

4) *Other rules of thumb.* The rule of equalizing primary and secondary winding losses is not correct. In the theoretical optimal design, they are 3.8 W for the primary and 4.2 W for the secondary. Another rule proposes to distribute equally the window area between primary and secondary windings. Although, in this case, it coincides with the optimal design, it does not work for non-interleaved

TABLE VIII OPTIMAL, DIFFERENT LITZ-WIRE SIZING, LOW-COST AND COMMERCIAL DESIGNS

Performance at rated power (τ_{amb} 45 °C)	***Practical-Optimal Design***	***Litz-wire 1*** $r_0=\delta$	***Litz-wire 2*** $r_0=\delta/3$	***Litz-wire 3*** $r_0=\delta/7$	***Litz-wire 4*** $r_0=\delta/20$	***Optimal Low-Cost Design*** Fig. 6	***Commercial Transformer*** Section V
a (mm)/$c1$/$c2$/$c3$	21.4/0.4/1.4/3.7	-	-	-	-	20/0.6/1.1/4.1	22/0.6/2/2.9
$m_p/m_s/b_p/b_s$	1/1/5/8	-	-	-	-	1/1/5/4	1/1/5/8
r_{0p}/r_{0s} (mm)	0.036/0.042	0.334	0.111	0.048	0.017	0.04/0.05	0.09
N_{0p}/N_{0s}	1594/740	20/14	175/110	913/571	23649/14781	1100/660	336/240
$(R_{dc,p}/R_{dc,s})_{100°C}$ (mΩ)	3.7/10.8	3.5/10.3	3.5/10.5	3.6/10.8	4.7/13.9	4.6/9.5	5.8/13.1
$(F_{ac,p}/F_{ac,s})_{50\ kHz}$	1.05/1.04	3.78/2.74	1.49/1.31	1.09/1.06	1/1	1.05/1.08	1.49/1.35
$(F_{ac,p}/F_{ac,s})_{150\ kHz}$	1.44/1.38	26.1/16.7	5.42/3.76	1.81/1.51	1.01/1.01	1.46/1.68	5.42/4.16
B_p (T)	0.127	-	-	-	-	0.13	0.077
V_e (dm^3)	0.295	-	-	-	-	0.287	0.420
τ_{ope}/ $\Delta\tau_{max}$ (°C)	97.5/52.5		106/61	97.7/52.7	102/57	100/55	101/56
P_w/P_c (W)	7/7.3	Non-feasible	9.6/7.2	7.3/7.3	8.4/7.2	7.6/7	13.9/2.1
P_{w50}/P_{w150} (W)	6.7/0.33		8.7/0.9	6.9/0.4	8.2/0.25	7.3/0.33	12.6/1.3
η (%)	99.71	0	99.66	99.70	99.69	99.70	99.68

windings [1]. Finally, only one magnetic material is usually considered for a given frequency range. As shown in [42], the borderline between different soft magnetic materials depends indeed on the specifications and cannot be generalized. The design methodology has taken into account all the available magnetic materials, being in this case the optimal one the N87 ferrite.

In order to observe the manufacturing environment constraints and minimize the cost, the optimal design must be implemented by using only commercially available materials. This commercial implementation of the optimal design, named optimal low-cost design, must maintain the optimal performance of the original design. With respect to the magnetic core, it is usually possible to achieve commercial core shapes similar to the optimal ones by combining standardized cores. The *c2* coefficient can be increased or decreased by combining E and U cores with I cores. Different values for *c3* can be achieved by stacking cores of the same type. On the contrary, dimensional factor *a* and *c1* coefficient are only available for the discrete values offered in the market. In this case, a combination of three EI65/32/27 cores of N87 ferrite leads to a core shape close to the optimal one. Regarding the conductors, a solution close to the optimal can be achieved with the next standardized round litz wires found in a commercial catalog [43]: 40 AWG diameter and 1100 strands for the primary and 38 AWG diameter and 660 strands for the secondary.

Finally, the performance of the low-cost design and the commercial prototype presented in Section V are shown in Table VIII. When comparing the optimal low-cost design to the commercial one, it must be noticed that the power density has risen from 11.9 kW/dm^3 to 17.4 kW/dm^3, which is a 46.5% increase, reaching even a higher efficiency that, at rated power, has risen from 99.68% to 99.70%. The window transversal section of the optimal low-cost design is shown in Fig. 6 at real size, with the primary winding blue colored and the secondary green colored.

IX. CONCLUSION

An analytical methodology for the design of power high-frequency litz-wired transformers has been presented in this paper. Existing models for the characterization of the transformer core and winding losses and its thermal resistance have been reviewed, evaluated and selected for their use in the design methodology. The proposed methodology comprehensively represents the multi-physical phenomena taking place in the electromagnetic device and makes it possible to understand the nature of the design problem, thus making easier the complex task of designing these magnetic devices. A design example for a 5 kW 50 kHz PV converter application has been carried out resulting in an optimal design with a power density of 17.4 kW/dm^3 and an efficiency at rated power of 99.70%. When compared to a commercial one, an increase of 46.5% in the power density is achieved.

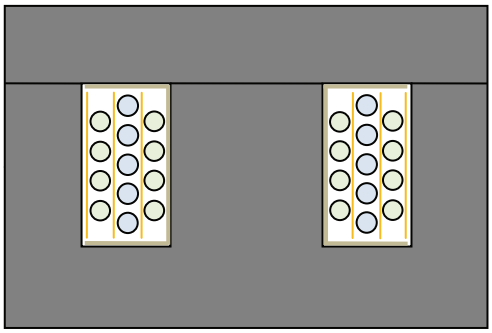

Fig. 6. Window transversal section of the optimal low-cost designs.

ACKNOWLEDGMENT

The authors gratefully acknowledge INGETEAM POWER TECHNOLOGY for their financial and permanent support.

REFERENCES

[1] R. Petkov, "Optimum design of a high-power, high-frequency transformer," *IEEE Trans. Power Electron.*, vol. 11, no. 1, pp. 33-42, Jan. 1996.

[2] U. Badstuebner, J. Biela, D. Christen, and J. W. Kolar, "Optimization of a 5-kW telecom phase-shift DC-DC converter with magnetically integrated current doubler," *IEEE Trans. Ind. Electron.*, vol. 58, no. 10, pp. 4736-4745, Oct. 2011.

[3] F. Krismer, and J. W. Kolar, "Efficiency-optimized high-current dual active bridge converter for automotive applications," *IEEE Trans. Ind. Electron.*, vol. 59, no. 7, pp. 2745-2760, Jul. 2012.

[4] B. Zhao, Q. Song, and W. Liu, "Experimental comparison of isolated bidirectional DC-DC converters based on all-Si and all-SiC power

devices for next-generation power conversion application," *IEEE Trans. Ind. Electron.*, vol. 61, no. 3, pp. 1389-1393, Mar. 2014.
[5] P. Xuewei, and A. K. Rathore, "Novel bidirectional snubberless naturally commutated soft-switching current-fed full-bridge isolated DC/DC converter for fuel cell vehicles," *IEEE Trans. Ind. Electron.*, vol. 61, no. 5, pp. 2307-2315, May 2014.
[6] H. Keyhani, H. A. Toliyat, M. Harfman-Todorovic, R. Lai, and R. Datta, "An isolated resonant AC-link three-phase AC-AC converter using a single HF transformer," *IEEE Trans. Ind. Electron.*, vol. 61, no. 10, pp. 5174-5183, Oct. 2014.
[7] B. Zhao, W. Song, W. Liu, and Y. Sun, "A synthetic discrete design methodology of high-frequency isolated bidirectional DC/DC converter for grid-connected battery energy storage system using advanced components," *IEEE Trans. Ind. Electron.*, vol. 61, no. 10, pp. 5402-5410, Oct. 2014.
[8] I. Villar, A. Garcia-Bediaga, U. Viscarret, I. Etxeberria-Otadui, and A. Rufer, "Proposal and validation of medium-frequency power transformer design methodology," in *Proc. IEEE ECCE*, 2011, pp. 3792-3799.
[9] P. Shuai, and J. Biela, "Design and optimization of medium frequency, medium voltage transformers," in *Proc. IEEE EPE*, 2013, pp. 1-10.
[10] E. I. Amoiralis, M. A. Tsili, D. G. Paparigas, and A. G. Kladas, "Global transformer design optimization using deterministic and nondeterministic algorithms," *IEEE Trans. Ind. Appl.*, vol. 50, no. 1, Jan./Feb. 2014.
[11] N. R. Coonrod, "Transformer computer design aid for higher frequency switching power supplies," *IEEE Trans. Power Electron.*, vol. PE-1, no. 4, pp. 248-256, Oct. 1986.
[12] E. C. Snelling, *Soft Ferrites: Properties and Applications*, 2nd ed. London, U.K.: Butterworths, 1988, ch. 11.
[13] W. G. Odendaal and J. A. Ferreira, "Effects of scaling high-frequency transformer parameters," *IEEE Trans. Ind. Appl.*, vol. 35, no. 4, pp. 932-940, Jul./Aug. 1999.
[14] N. Mohan, T. M. Undeland, and W. P. Robbins, *Power Electronics: Converters, Applications, and Design*, 3th ed. New York, NY: John Wiley & Sons, Inc., 2003, ch. 29-30.
[15] C. W. T. McLyman, *Transformer and Inductor design Handbook*, 3th ed. New York, NY: Marcel Dekker, Inc., 2004, ch. 5-7.
[16] F. Forest, E. Labouré, T. Meynard, and M. Arab, "Analytic design method based on homothetic shape of magnetic cores for high-frequency transformers," *IEEE Trans. Power Electron.*, vol. 22, no. 5, pp. 2070-2080, Sept. 2007.
[17] Z. Ouyang, O. C. Thomsen, and M. A. E. Andersen, "Optimal design and tradeoff analysis of planar transformer in high-power dc-dc converters," *IEEE Trans. Ind. Electron.*, vol. 59, no. 7, pp. 2800-2810, Jul. 2012.
[18] W. G. Hurley, and W. H. Wölfle, *Transformers and Inductors for Power Electronics: Theory, Design and Applications*, 1st ed. Chischester, U.K.: John Wiley & Sons, Ltd., 2013, ch. 4, 5.
[19] A. De Nardo, G. Di Capua, and N. Femia, "Transformer design for isolated switching converters based on geometric form factors of magnetic cores," *IEEE Trans. Ind. Electron.*, vol. 60, no. 6, pp. 2158-2166, Jun. 2013.
[20] M. K. Kazimierczuk, *High-Frequency Magnetic Components*, 2nd ed. Chischester, U.K.: John Wiley & Sons, Ltd., 2014, ch. 11.
[21] Steinmetz, C. P., "On the law of hysteresis", *Proc. IEEE*, vol. 72, no. 2, pp. 197–221, Feb. 1984.
[22] S. A. Mulder, "Fit formulae for power loss in ferrites and their use in transformer design," in *Proc. PCIM*, 1993, pp. 345–359.
[23] I. Villar, U. Viscarret, I. Etxeberria-Otadui, A. Rufer, "Global loss evaluation methods for nonsinusoidally fed medium-frequency power transformers," *IEEE Trans. Ind. Electron.*, vol. 56, no. 10, pp. 4132-4140, Oct. 2009.
[24] J. Mühlethaler, J. Biela, J. W. Kolar, and A. Ecklebe, "Improved core-loss calculation for magnetic components employed in power electronic systems," *IEEE Trans. Power Electron.*, vol. 27, no. 2, pp. 964-973, Feb. 2012.
[25] J. Lammeraner and M. Stafl, *Eddy Currents*. 1st ed. London, U.K.: Iliffe Books, Ltd., 1966, ch. 7.
[26] C. R. Sullivan, "Computationally efficient winding loss calculation with multiple windings, arbitrary waveforms, and two-dimensional or three-dimensional field geometry," *IEEE Trans. Power Electron.*, vol. 16, no. 1, pp. 142-150, Jan. 2001.
[27] H. Hämäläinen, J. Pyrhönen, J. Nerg, and J. Talvitie, "AC resistance factor of litz-wire windings used in low-voltage high-power generators," *IEEE Trans. Ind. Electron.*, vol. 61, no. 2, pp. 693-700, Feb. 2014.
[28] X. Nan, and C. R. Sullivan, "An equivalent complex permeability model for litz-wire windings," *IEEE Trans. Ind. Appl.*, vol. 45, no. 2, pp. 854-860, Mar. 2009.
[29] C. R. Sullivan, "Optimal choice for number of strands in a litz-wire transformer winding," *IEEE Trans. Power Electron.*, vol. 14, no. 2, pp. 283 -291, Mar. 1999.
[30] R. P. Wojda, and M. K. Kaizimierczuk, "Winding resistance of litz-wire and multi-strand inductors," *IET Power Electron.*, vol. 5, iss. 2, pp. 257-268, Feb. 2012.
[31] M. Bartoli, N. Noferi, A. Reatti, and M. K. Kazimierczuk, "Modeling litz-wire winding losses in high-frequency power inductors," in *Proc. IEEE PESC,* 1996, pp. 1690-1696.
[32] F. Tourkhani and P. Viarouge, "Accurate analytical model of winding losses in round litz wire windings," *IEEE Trans. Magn.*, vol. 37, no. 1, pp. 538–543, Jan. 2001.
[33] P. L. Dowell, "Effects of eddy currents in transformer windings," *Proc. Inst. Elect. Eng.*, vol. 113, pp. 1387-1394, Aug. 1966.
[34] J. A. Ferreira, "Improved analytical modeling of conductive losses in magnetic components," *IEEE Trans. Power Electron.*, vol. 9, no. 1, pp. 127-131, Jan. 1994.
[35] C. Buccella, C. Cecati, and F. de Monte, "A coupled electrothermal model for planar transformer temperature distribution computation," *IEEE Trans. Ind. Electron.*, vol. 55, no. 10, Oct. 2008.
[36] EPCOS AG. (2006). Application notes. Ferrites and accessories. [Online]. Available: http://www.epcos.com/
[37] E. L. Barrios, A. Ursúa, L. Marroyo, and P. Sanchis, "Modelling, improvement and experimental validation of a 50 kHz-5 kVA litz-wired transformer for PV inverters," in *Proc. IEEE ECCE*, 2013, pp. 4364-4371.
[38] PACK Feindrähte. (2013). Technical Data. RUPALIT® high-frequency litz wires. [Online]. Available: http://www.pack-feindraehte.de/
[39] F. de León, S. Purushothaman, and L. Qaseer, "Leakage inductance design of toroidal transformers by sector winding," *IEEE Trans. Power Electron.*, vol. 29, no. 1, pp. 473-480, Jan. 2014.
[40] M. Borage, K. V. Nagesh, M. S. Bhatia, and S. Tiwari, "Design of LCL-T resonant converter including the effect of transformer winding capacitance," *IEEE Trans. Ind. Electron.*, vol. 56, no. 5, May 2009.
[41] A. Ayachit and M. K. Kazimierczuk, "Thermal effects on inductor winding resistance at high frequencies," *IEEE . Magn. Lett.*, vol. 4, pp. 0500304, Sept. 2013.
[42] G. Ortiz, M. Leibl, J. W. Kolar, and O. Apeldoorn, "Medium frequency transformers for solid-state-transformer applications – Design and experimental verification," in *Proc. IEEE PEDS*, 2013, pp. 1285-1290.
[43] New England Wire Technologies. (2013). Product Selection Guide. [Online]. Available: http://newenglandwire.com/newt-catalog.pdf
[44] C. R. Sullivan, "Cost-constrained selection of strand wire and number in a litz-wire transformer winding," *IEEE Trans. Power Electron.*, vol. 16, no. 2, pp. 281-288, Mar. 2001.

Ernesto L. Barrios (S'12) was born in Pamplona, Spain, in 1988. He received the B.Sc. and M.Sc. degrees (with honors) in Electrical Engineering from the Public University of Navarre, Pamplona, Spain, in 2009 and 2012, respectively.

In 2011, he joined the Research Group in Electrical Engineering, Power Electronics and Renewable Energy (INGEPER) of the Public University of Navarre, where he is currently pursuing his Ph.D. His main research interests include high frequency magnetics, wide bandgap power semiconductor devices and power converters for renewable energies, particularly for photovoltaics and fuel cells.

Alfredo Ursúa (M'04) received the B.Sc. and M.Sc. degrees, both with honors, in Electrical Engineering in 2001 and 2004, respectively, and the Ph.D. degree in Electrical Engineering in 2010, all from the Public University of Navarre, Spain.

In 2002 he joined the Department of Electrical and Electronic Engineering at the Public University of Navarre, first as a researcher and since 2010 as Associate Professor. He is member of the Steering Committee of the university Chair for Renewable

Energies and has been involved in several research projects both with private and public funding, and mainly related to renewable energy systems, hydrogen technologies, power electronics and electric microgrids. He has also co-authored more than 45 journal papers and conference contributions, and holds 2 patents.

Dr. Ursúa is member of the IEEE and the Spanish Hydrogen Association.

Luis Marroyo (M'04) received the M.Sc. degree in electrical engineering in 1993 from the University of Toulouse, France, and the Ph.D. degree in electrical engineering in 1997 from the Public University of Navarre (UPNa), Spain, and in 1999 from the LEEI-ENSEEIHT INP Toulouse, France.

From 1993 to 1998, he was Assistant Professor at the Department of Electrical and Electronic Engineering of the UPNa, where he currently works as Associate Professor, since 1998. He is the head of the Electrical Engineering, Power Electronics and Renewable Energy research group (INGEPER). He has been involved in more than 60 research projects mainly, in co-operation with industry, he is the co-inventor of 11 international patents and co-authored of more than 70 papers in international journals and conferences. His research interests include power electronics, grid quality and renewable energy.

Pablo Sanchis (M'03, SM'12) received the M.Sc. and Ph.D. degrees (with honors) in Electrical Engineering in 1995 and 2002, respectively, and the M.Sc. degree in Management and Business Administration in 1994, all from the Public University of Navarra, Pamplona, Spain.

From 1996 to 1998, he worked as a Guest Researcher at Delft University of Technology, The Netherlands. In 1998, he joined the Department of Electrical and Electronic Engineering at the Public University of Navarra, where he is currently Associate Professor. He is also Director of the Chair for Renewable Energies of the university, and Vice Dean of the Technical School for Industrial Engineering and Telecommunications.

He has been involved in more than 62 research projects mainly in co-operation with industry, and is the co-inventor of 8 patents. He has also co-authored 32 journal papers and more than 60 conference contributions. Dr. Sanchis is member of IEEE, CIGRE and the Spanish Hydrogen Association. His research interests include renewable energies, power electronics, hydrogen technologies, electric grid integration and electric microgrids.